



Laser-patterned carbon coatings on flexible and optically transparent plastic substrates for advanced biomedical sensing and implant applications

Journal:	<i>Journal of Materials Chemistry C</i>
Manuscript ID	TC-ART-10-2021-005176.R1
Article Type:	Paper
Date Submitted by the Author:	28-Dec-2021
Complete List of Authors:	Joshi, Pratik; NCSU, Materials Science and Eng. Riley, Parand; North Carolina State University Denning, Warren; Anton Paar USA Shukla, Shubhangi; North Carolina State University Khosla, Nayna; North Carolina State University Narayan, Jagdish; North Carolina State University Narayan, Roger; University of North Carolina at Chapel Hill,

Laser-patterned carbon coatings on flexible and optically transparent plastic substrates for advanced biomedical sensing and implant applications

Pratik Joshi¹, Parand R. Riley¹, Warren Denning², Shubhangi Shukla³, Nayna Khosla¹, Jagdish Narayan¹, Roger Narayan^{1,*}

¹ Department of Materials Science and Engineering, North Carolina State University, Raleigh, NC 27695-7907 USA

² Anton Paar USA, Inc., 10215 Timber Ridge Drive, Ashland, VA 23005 USA

³ Joint Department of Biomedical Engineering, North Carolina State University, Raleigh, NC 27695-7907 USA

*Corresponding Author E-mail: narayan@ncsu.edu (Jagdish Narayan), rjnaraya@ncsu.edu (Roger Narayan)

Abstract

Medical grade polyethylene-based skeletal implants exhibit osteo-disintegration, erosion, and modest hemocompatibility. Herein, we report on the fabrication of highly adherent undoped and Si-containing DLC (Si-DLC) coatings for biomedical implant applications by utilizing plasma and laser-based processing techniques on thermally sensitive polyethylene (PE) substrates. Scratch testing reveals a strong interfacial shear strength of 620 MPa for DLC coatings deposited on PE. A contact stress of ~ 32 MPa induced cracking of DLC thin film. The Si-DLC films demonstrated a higher critical failure load and less cracking compared to undoped DLC films. The contact angle for PE increased from 90° to 110° when it was coated with the Si-DLC thin film. A high optical bandgap of 2.5 eV was calculated for the 21 at% Si-DLC thin films. Pulsed laser annealing (PLA) of Si-DLC films at 0.3 J cm^{-2} increased the amount of sp^2 bonded carbon, resulting in an improvement in lubricity, hydrophobicity, and electrical conductivity properties. In addition, the laser patterned pristine DLC films showed the formation of reduced graphene oxide, which possessed sizeable properties for wearable electronics and biosensing applications ($R_s = 0.6 \text{ k}\Omega/\square$). This study indicates that PLA is a useful technique for modifying the properties of DLC thin films on flexible polymeric substrates for state-of-the-art biomedical and electronic sensing applications.

Keywords: Adhesion, Biomedical, flexible electronics, reduced graphene oxide

I. Introduction

Ease of availability, low cost, recyclability, high chemical resistance, and biocompatibility make polyethylene (PE) and its derivatives an appropriate substrate material for continuous health monitoring devices, thin electronic devices/displays, and biomedical implant applications¹. The ability of PE to exist in versatile forms like high-density polyethylene (HDPE), ultra-high molecular weight polyethylene (UHMWPE), highly cross linked polyethylene (HXLPE), low-density polyethylene (LDPE) makes it possible to obtain desired optical and mechanical properties. Metallic implants often suffer from complications such as fracture and metal ion release. Hence, the replacement of conventional metallic implants with PE is a topic of substantial research. Currently, the Medial Cup® acetabular implant from Aston Medical, the Boubella-E esophageal stent from ELLA-CS, and many other FDA-approved medical devices make use of PE². However, almost all forms of PE suffer from two major drawbacks, poor wear resistance and thermal conductivity; these factors significantly limit the use of PE for medical applications. For example, UHMWPE hip implants show poor wear resistance when exposed to cyclical contact stresses at the articular surface. Wear particles of approximately 0.7 μm in size are produced, which may induce adverse tissue reactions³. Notably, DLC coatings exhibit good biocompatibility, which is associated with their chemical inertness⁴. DLC-coated UHMWPE implants exhibited reduced wear and showed better antimicrobial properties compared to hydroxyapatite-coated UHMWPE⁵⁻⁸. However, the adhesion of conventional DLC coatings on HDPE has not been satisfactory; a DLC-coated HDPE joint replacement was withdrawn shortly after introduction due to coating delamination and high rates of HDPE wear⁹⁻¹¹.

PE and its derivatives are also widely used as substrates in flexible electronic applications. The ongoing miniaturization of flexible electronics is expected to be associated with severe polymer substrate heating, resulting in reduced service lifetimes for sensors and other electronic devices¹². In this context, a reduced graphene oxide coating on flexible electronic device substrates can act as a thermal sink and an electrical conductor. It may also act as a barrier layer to protect the substrate from moisture absorption; in addition, it can be utilized for catalytic sensing via enzymatic and non-enzymatic mechanisms¹³⁻¹⁷. Currently, high quality reduced graphene oxide (rGO) can be produced by thermal or chemical reduction of graphene oxide (GO). The conventional furnace-based thermal reduction of GO approach is problematic as it exposes the entire device to high temperatures, leading to substrate degradation. In addition, the

approach that involves fabricating high-quality graphene on a separate metallic substrate such as Cu and then transferring it onto a flexible polymeric substrate is associated with significant structural damage during the film transfer process. Currently, chemical-based reduction of GO is the only method shown to be useful for local fabrication of rGO on polymeric substrates since the chemical reduction is usually carried out under milder conditions¹⁸. In many cases, the chemicals used for reduction are toxic; as such, this approach is not feasible for mass production. Researchers have previously fabricated the Q-carbon (sp^3 rich) phase of carbon and laser-induced reduced graphene oxide (LIRGO) thin films (sp^2 rich) by melting amorphous carbon with nanosecond (ns) excimer pulses on sapphire and silicon substrates¹⁹⁻²². This method can further be extended towards flexible polymeric substrates as the heat flow in ns laser-based rapid thermal processing is spatially and temporally confined. Notably, the high selectivity of excimer lasers towards amorphous carbon (a-C) thin films, which exhibit low bandgap and high absorptivity compared to PE substrates, results in high-quality rGO film synthesis without any substrate heating or degradation²³.

The amount of sp^2 and sp^3 bonding in carbon films has a substantial effect on their mechanical, electronic, and thermal properties²⁴⁻²⁶. Si doping in DLC promotes sp^3 bonding, leading to reduced stress in the thin film. It also has useful effects on hemocompatibility, cell proliferation, and antibacterial resistance^{27,28}. Recent studies indicate that films with a Si content of ~21 at% show appropriate in vitro biocompatibility properties with endothelial cells²⁹. In this study, we report a novel approach to tailor the adhesion, hydrophobicity, and electrical conductivity of DLC coatings on HDPE substrates. This approach was achieved by fabricating Si-containing DLC (Si-DLC) coatings using PECVD and undoped DLC coatings after fluorine-reactively ion etching (F-RIE) by PLD. This study considered the usage of carbon-coated HDPE substrates for biomedical implant and electrical sensing applications. For biomedical implant applications, adhesion and biocompatibility are critical; adhesion and high electrical conductivity are essential for electrical sensing applications. Initially, the improvement in adhesion with and without Si doping in the DLC film was investigated using a scratch adhesion test. Further, the biocompatibility of 21 at% Si-DLC films was assessed using contact angle measurements. Finally, for making the films conductive, we laser irradiated both the undoped and Si-containing DLC thin films to form LIRGO and studied the electrical behavior of these films as a function of energy density.

II. Experimental procedure

a) Plasma cleaning and thin film deposition

1) RIE and PLD

Plasma treatment was performed by using a Plasmalab 80 Plus reactive ion etcher (RIE) (Oxford Instruments, Tubney Woods, Abingdon, UK) to render the surface fluorine terminated. A gas flow of 25 sccm Ar and 25 sccm CHF₃ with a working pressure of 50 mTorr and a power of 50 W for 1 minute was applied. The power and duration of the treatment were chosen to minimize the etching of the film. 250 nm amorphous carbon thin films were deposited using PLD at a vacuum of 1×10^{-6} Torr by utilizing KrF excimer laser shots to irradiate a glassy carbon target at a frequency of 10 Hz.

2) PECVD

A custom-designed PECVD instrument was used to deposit Si-DLC thin films on HDPE substrates as described by Sakhrani^{30,31}. The thin film deposition process consisted of three steps: a) substrate loading, b) cleaning the substrate, and c) deposition of the Si-DLC thin film on the substrate. During loading, the HDPE substrates were mounted onto a stainless steel plate. This plate was placed on the PTFE base plate electrode to electrically insulate it from the rest of the chamber. The chamber was pumped down overnight to achieve a base pressure of 1×10^{-8} Torr. After the loading stage, the cleaning of the substrate was carried out by simultaneously flowing Ar (90 sccm) and O₂ (50 sccm) gases and striking a plasma by applying radiofrequency (RF) power (13.56 MHz) to the large base electrode connected to an RFX-600 power supply (Advanced Energy, Denver, CO) in the process chamber for 10 minutes. The plasma was kept stable by not letting the reflective power go above 10 W using a matching network system. An oscilloscope (Aligent, Santa Clara, CA) was used to measure the peak to peak voltage (V_{pp}). For cleaning, a V_{pp} of 400 mV was utilized. The rest of the chamber was electrically grounded. The process gases were uniformly released into the chamber from the showerhead distribution ring that was located at the top of the chamber. Over the course of two minutes, Ar, O₂, and tetramethylsilane (1.6 sccm) gases entered the chamber; the V_{pp} decreased to 300 mV peak to peak. After two minutes, the flow of O₂ was stopped. It is surmised that an O₂ flow for two minutes at the start of deposition is helpful to improve film adhesion. The thin film deposition process was carried out for one hour. After one hour, the chamber was subjected to an Ar gas purge before chamber venting.

3) PLA

Pulsed laser annealing of DLC and Si-DLC thin films was carried out using an ArF laser (193 nm). The laser was focused with the help of a plano-convex lens that was capable of producing an energy density in the range of 0.1-1.6 J/cm². The energy was measured using the MAX mol meter. The spot size could be adjusted by changing the distance between the sample being irradiated and the laser source.

b) Characterization

i) HRSEM, Raman, FTIR, AFM and UV-Vis

The as-deposited films and films after laser annealing were characterized using an Alpha Raman spectroscopy instrument (WITec, Ulm, Germany) at wavelengths 514 and 632 nm. The film microstructure was assessed using a Verios 460L scanning electron microscope (FEI, Hillsboro, OR). Surface morphology and roughness of the DLC thin films were examined by an MFP-3D Origin+ atomic force microscope (Asylum Research, Santa Barbara, CA), which was equipped with Budget Sensors Multi tip in tapping mode using a resonant frequency of approximately 50 kHz, a scan size of 10 μm x 10 μm, and a scan rate of 0.75 lines per second.

The surface elemental composition and sp²/sp³ content of carbon films were analyzed using SPECS FlexMod X-ray photoelectron spectroscopy instrument that utilized an Mg K_α (1254 eV) excitation source with a PHOIBIS 150 hemispherical analyzer (SPECS Surface Nano Analysis GmbH, Berlin, Germany). The spectra were calibrated using the spectrum for adventitious carbon, a C 1s line located at 285 eV.

Fourier transform infrared spectra were obtained using an ALPHA instrument (Druker, Billerica, MA), which is capable of a resolution of 4 cm⁻¹ and an absorbance data range of 400 to 4000 cm⁻¹. The UV-Vis spectra of the samples were characterized using a UV-1800 UV-visible spectrometer (Shimadzu, Kyoto, Japan) in the wavelength range from 300 to 1100 nm; this instrument provides a resolution of 1 nm.

ii) TEM

High-resolution transmission electron microscopy (HRTEM) imaging, electron diffraction, and energy-dispersive X-ray analysis (EDS) were acquired using a Talos-F200 microscope (FEI, Hillsboro, OR) with an 'XFEG' Schottky field emission gun source at 80 keV; an objective aperture was used to obtain good contrast and weaken the beam to prevent charging. The samples were glued between two pieces of polystyrene with superglue and allowed to dry overnight.

Sections were cut with a Diatome diamond knife on a UC7 ultramicrotome (Leica, Wetzlar, Germany) at three different thicknesses: 120 nm, 110 nm, and 100 nm.

iii) Contact angle, adhesion, and electrical measurements

The sessile drop method was utilized in this study; a deionized water drop was placed on the tested surfaces. An OCA 15EC optical contact angle meter (Dataphysics Instruments GmbH, Germany) was used to record the contact angle data. The drop age range for the calculation was 4.9-5.1 seconds, and the drop volume was ~0.2 microliter.

The adhesion of coatings was examined using a micro scratch instrument (Anton Paar, Graz, Austria). A diamond spheroconical indenter with a 10 μm tip radius was used for the measurements. The stylus was moved at a constant speed of 1.2 mm/s during the micro scratch studies. The loading rate along the direction normal to the substrate was 2 mN/s.

The sheet resistivity measurements were performed using a Model RM3-AR instrument (Jandel, Leighton Buzzard, United Kingdom.) connected to a four-point probe setup. The current range of this device was 10 nA-1mA. The measurements were performed in both forward and reverse directions to confirm the stability of the film and validate the results. The instrument was calibrated with a 100 Ω resistor before performing any measurements.

III. Results and discussion

Figure 1 depicts the schematic representation of the different methods used to deposit and modify the structure of DLC thin films on HDPE substrates in this study. The DLC deposited on as-received HDPE using PLD resulted in delamination upon minor bending or twisting of the substrate. Hence, fluorine-based RIE (F-RIE) was conducted on HDPE substrates; these substrates were then coated with DLC thin films in the PLD system (Fig. 1 (a)). This film was later annealed at 0.3 J cm^{-2} , which results in rGO formation. For Si-doped DLC thin film deposition on HDPE, a PECVD system was utilized. The thin films were translucent, with a slight yellowish color (Fig. 1(b)). The HDPE-coated Si-DLC system demonstrated high flexibility without delamination. Finally, the Si-DLC thin films were subjected to PLA at energy densities of 0.1-1 J/ cm^2 ; its effect on material properties was studied (Fig. 1(c)).

Figure 2 shows the Raman spectra and XRD data from as-received HDPE. The Raman spectrum at 632 nm shows the presence of C-C (1000-1250 cm^{-1}) and CH_2 twist modes. The CH_3 - CH_2 overtone peak is visible at ~2945 cm^{-1} (Fig. 2(b)). Additional peaks near 2945 cm^{-1} were attributed to Fermi resonance between the CH_2 symmetric stretching and the overtone from the CH_2 bonds. The CH_2 bending mode occurs at 1416 and 1440 cm^{-1} . The C-H stretching peaks fall in the

range of 2825 and 2970 cm^{-1} ³². HDPE exhibits sharp peaks at 1445 cm^{-1} and 1421 cm^{-1} as well as bands at 1299, 1132, and 1067 cm^{-1} due to the trans $-(\text{CH}_2)_r-$ group as observed in Figure 2(a)^{33 34}. The XRD peak for unmodified HDPE was observed at 21°, corresponding to the (110) plane with the orthorhombic crystal structure; this (110) broad peak also overlapped with the (200) peak (Fig. 2(c)). Figure 2 (d) shows the delamination of DLC coating on untreated HDPE after laser annealing at 0.1 J cm^{-2} , indicating poor film adhesion.

1. Adherent DLC coatings for biomedical implant applications

The failure stress for films on flexible substrates is given by the Stoney equation: $\sigma_f = \frac{E_s d_s^2}{6R(1-\nu_s)d_f}$. In this equation, R is the radius of curvature, d_s is substrate thickness, d_f is film thickness, and ν_s is Poisson's ratio of substrate³⁵. When $d_s \gg d_f$, the peak film strain as a function of curvature is given by $\varepsilon_f = \frac{d_s}{2R}$. For HDPE of $\sim 100 \mu\text{m}$ thickness and assuming a failure strain for typical brittle films of 0.5-1%, a maximum bending radius of only 5 mm is possible before film failure. Notably, the properties of DLC thin films are reported to be considerably different on polymeric substrates than on other substrates³⁶.

(a) Fabrication of pristine DLC coatings on F-RIE HDPE substrate by PLD

Researchers have previously tried to deposit DLC films on HDPE by vacuum pulsed sputtering³⁷. The low melting temperature of HDPE is incompatible with techniques that are associated with high substrate temperatures for improved film adhesion. Trakhtenberg et al.³⁸ showed that a substrate temperature close to the melting point of HDPE increases the adhesion of DLC thin films to PE substrates. Several studies have considered the development of methods to improve the adhesion properties of coatings on PE substrates, including plasma and primer treatment

Figure. 3 shows a comparison of the HDPE surface before and after RIE treatment. The as-received HDPE shows very high roughness and an uneven surface. Even the smoothest of regions show the presence of pits exceeding 25 nm in depth (Fig. 2(e)). The depth of the pits is uneven. The RMS roughness value was $5.61 \pm 4.27 \text{ nm}$. After RIE, the surface was relatively smooth with sufficient roughness to promote film adhesion. Even in the roughest of the regions, the pit depth is not more than 15 nm. The RMS roughness value calculated was $3.78 \pm 2.58 \text{ nm}$. The parameters for F-RIE were selected such that etching, as well as surface fluorination, took place simultaneously³⁹⁻⁴¹. Since fluorine is surface-active, it forms C-F bonds and improves the adhesion of the thin film⁴². As discussed earlier, the AFM scan reveals the presence of small pits, cracks, and pores present on the as-received substrate surface. The high standard deviation observed in the surface

roughness measurement also indicates the presence of defects in the substrate. This phenomenon leads to decreased adhesion of DLC films on these substrates. During the film deposition process, the DLC film follows the characteristics of the substrate surface, leading to non-uniform film deposition and film cracking due to the brittle nature of these films. During RIE, the etching rates of the amorphous regions and crystalline regions of PE differ, resulting in an increase in non-uniform regions and pit formation. The defective and deep pit regions are ideal for grafting fluorine-containing functionalities obtained from highly reactive CF_x radicals, making the surface highly reactive while maintaining uniform surface roughness⁴¹. The dangling bonds present on the surface and uniform surface roughness result in improved film adhesion.

Figure 4 shows the Raman spectrum and an optical micrograph of the scratch test result from an as-deposited DLC thin film on HDPE. Figure 4(a) reveals the Raman spectrum of DLC deposited on HDPE with (blue) and without (red) F-RIE treatment. The stress present in the DLC thin film can be calculated from the G peak shift⁴³. Stress-free DLC thin films show a G peak in the range 1545-1560 cm^{-1} . The as-deposited DLC thin film without RIE treatment on HDPE shows a G peak at $\sim 1583\text{ cm}^{-1}$, indicating substantial compressive stress ($>8\text{ GPa}$). The DLC thin film on RIE treated HDPE shows a G peak at $\sim 1572\text{ cm}^{-1}$, indicating a decrease in the stress of at least 2 GPa compared to non-treated HDPE. These results suggest that DLC deposited after F-RIE should possess higher adhesion as compared to the non-treated HDPE. Since the coating thickness is the same for both thin films ($\sim 250\text{ nm}$), scratch testing can be used to obtain semi-quantitative comparisons⁴³. We have performed progressive load scratch tests for adhesion assessment of DLC-coated HDPE by PLD with and without F-RIE. In progressive load scratch testing, the tip load increases at a constant rate as the tip progresses along the scratch path. To distinguish between different failure types, we report two loads (L_{c1} and L_{c2}). L_{c1} is taken as the load at which cohesive failure modes (e.g., cracking, chipping of the coating) occur; L_{c2} is the load corresponding to the onset of adhesive failure (i.e., the load at which the substrate is first exposed)⁴⁴. The significances of L_{c1} and L_{c2} depend on the application of the thin film; one type can be more important than the other for a given application. For example, a DLC thin film on a drill bit may be considered failed when the substrate underneath is exposed as the drill bit would still function with a small chip (i.e., L_{c2} is the important parameter). If we consider a DLC thin film on a hip implant, failure is defined as the point where the thin film begins to delaminate, which introduces undesirable material into the body; thus, L_{c1} is the parameter of interest. For the DLC thin film deposited on HDPE without RIE adhesive failure (i.e., delamination was observed) at the start of the test, scratch testing was performed on bare HDPE; hence, 0.2 mN was the

critical load for coating removal (Fig. 4(b)). DLC thin films are brittle due to the lack of dislocation generation during deformation. The HDPE substrate has low hardness compared to the DLC coating; as such, tensile and Hertzian cracking along the direction of the scratches were observed along the scratch trace (Fig. 4(c)). For the DLC thin film deposited on HDPE with RIE, an initially cohesive failure (i.e., cracking and chipping) was observed. The value of L_{c1} noted was ~ 8.2 mN. After a load of 10 mN (L_{c2}), the substrate was visible. The interfacial shear strength of film is given by⁴⁵:

$$\tau_o = \frac{L_{c2}}{\pi a \sqrt{R^2 - a^2}} \quad (1)$$

Here, L_c is the critical load at which cracks begin to appear homogeneously, and a is the half-width of the track left after the test. The value of τ_o was determined to be 620 MPa for the DLC thin film on HDPE after F-RIE.

(b) Si-containing DLC coatings deposited by PECVD

The plasma-enhanced CVD (PECVD) process produces adherent DLC coatings on polymeric substrates since it introduces energy to the chemical reaction through plasma, enabling thin film deposition at lower temperatures. Recently, it was discovered that DLC layers on polyurethane obtained by the PECVD method were characterized by poor adhesion strength; pre-treating in an oxygen plasma improved adhesion⁴⁶. Hence, we have used the oxygen pretreatment approach for Si-DLC film deposition on the HDPE substrate.

Figure 5 illustrates the characteristics of a Si-DLC thin film deposited by PECVD on HDPE. The HRSEM image of the 500 nm Si-DLC thin film is illustrated in Fig. 5(b); 5-10 nm-sized grains were observed. Catena et al. observed 100 nm-sized grains in DLC thin films deposited on HDPE⁴⁷. AFM was used to evaluate the surface roughness of 200 nm Si-DLC thin films on HDPE substrate. The microscopic roughness profile also showed the presence of grains distributed evenly throughout the surface (Fig. 5(d, e)). The average height of these grains was found to be ~ 71 nm (Fig. 5(f)). The non-doped stress-free DLC thin films demonstrate signature Raman D and G peaks indexed at 1350 cm^{-1} and 1559 cm^{-1} , respectively. Si incorporation in DLC thin film increased the sp^3 bonding as the Si substitutes for a carbon site. Since the Si-C bond length is 1.89 \AA and the C-C bond length of 1.54 \AA , a long-range reduction in internal stress was observed⁴⁷. The Raman spectrum of the Si-DLC thin film shows a G peak at 1460 cm^{-1} (Fig. 5(c)).

Figure 6 shows a TEM image of a Si-DLC thin film on HDPE. Fig. 6(a) shows the low magnification image of the sample configuration. The coated HDPE was further attached to the polystyrene backing film with superglue to maintain

thin film integrity during sample preparation. The DLC thin film and superglue top layer are visible in Fig. 6(b). The DLC thin film appears with a dark color. Fig. 6 (c) contains an energy dispersive spectroscopy (EDS) spectrum that was acquired at the HDPE/Si-DLC interface. The HDPE shows the presence of carbon and no silicon, and the Si-DLC thin film shows the presence of Si (~21 wt%). The boundary between the Si-DLC thin film and the HDPE is very sharp. The small curvature that appears in the HDPE substrate is well accommodated by Si-DLC thin film, indicating strong adhesion. The Si-containing DLC thin film showed no signs of cracks and porosity. Fig. 6(d) shows the selected area diffraction pattern of the Si-DLC thin film. The amorphous structure shows strong (111) and (220) rings that correspond to a d spacing of 2 and 1.2 Å, which is characteristic of DLC thin films⁴⁸. The TEM result indicates minimal or no diffusion of Si from the thin film to the substrate. Fischer et al.³² have suggested the possibility of interlayer formation between the DLC thin film and PE with NEXAFS spectroscopy. However, no reports have studied the interlayer, thin-film porosity, and the interfacial region.

Adhesion testing was performed on Si-DLC thin films by applying a progressively increasing load. The adhesion of DLC thin films deposited on HDPE by PLD and PECVD with a similar thickness (~250 nm) was compared (Table 1). Cracking of the Si-DLC thin-film perpendicular to the scratch test direction was observed after the critical load (Fig. 7(a)). However, the cracking/chipping was less for the Si-DLC thin film than for the non-doped DLC thin film, suggesting an improvement in toughness of the thin film after Si incorporation; this result is in agreement with previous studies. The scratch test result from the laser annealed Si-DLC thin film is shown in Fig. 7(b). Interestingly, no cracking or delamination was observed until an applied load of 100 mN. This result suggests that the graphitic content in Si-DLC thin film has increased upon laser annealing, which has favorable effects on film toughness. Fig. 7(c) shows the contact angle values of HDPE, HDPE coated with Si-DLC and Si-DLC after laser annealing. The contact angle of HDPE was 90°, which is in agreement with previously observed values⁴⁹. However, we noted a sharp increase in the contact angle value after coating the HDPE with a 200 nm Si-containing DLC thin film. The increase in the contact angle value can be partly attributed to the relatively high roughness of the Si-DLC thin film. Surfaces with significantly low wettability are promising candidates for several biomedical applications⁵⁰⁻⁵². For instance, hydrophobic surfaces can show antithrombotic properties by facilitating the blood flow and reducing the shear stress between the solid and liquid interface³⁶⁻³⁷. They can also exhibit antimicrobial, self-cleaning, and anti-biofouling properties since the low adhesive forces and rough topographies reduce the contact area between an implant and its surroundings⁵³. For example, DLC-

modified HDPE is utilized in coronary stents due to its antithrombotic properties⁵⁴. The sp^2 and sp^3 content of a hard carbon surface affect its contact angle value. The sp^2 rich surface is known to show a higher contact angle than an sp^3 rich surface as the sp^3 terminated surface exhibits a strong covalent character⁵⁴.

Fig. 7 (e) contains the FTIR spectra for annealed and non-annealed Si-DLC thin films. The absorption band centered at $\sim 2900\text{ cm}^{-1}$ is typically displayed by hydrogenated amorphous carbon⁵⁵. The 2920 cm^{-1} peak is assigned to sp^3 CH and sp^3 CH₂ asymmetric bond stretching. The DLC thin film also exhibits peaks associated with C-CH₃ at 1370 and 1450 cm^{-1} . The large area under the peaks from $2700\text{-}3000\text{ cm}^{-1}$ after laser annealing confirms the higher amount of hydrogen in the thin film after laser annealing. The peak at 1055 cm^{-1} is very prominent in the laser annealed DLC thin film, indicating the presence of C-O⁵⁶ and Si-O groups⁵⁷. Fig. 6(f) contains an SEM micrograph of the laser annealed Si-DLC thin film; it shows the formation of SiO_x/graphitic carbon on the surface, which indicates that oxygen absorption occurred after laser annealing.

2. Patterned laser-induced rGO for flexible electronic sensing applications

(a) Electrical properties of as-deposited and laser annealed non-doped DLC coatings

Utilizing a metal shadow mask, we have further laser patterned reduced graphene oxide on a flexible F-RIE polyethylene substrate (Fig. S1 (a)). The laser patterning was carried out at an energy density of 0.3 J/cm^2 . The laser patterned regions showed the formation of rGO with an XRD peak at $\sim 25.5^\circ$ (Fig 8 (a)). The formation of rGO was also confirmed with Raman spectroscopy (Fig 8 (c)). The D and G peaks centered at 1340 and 1600 cm^{-1} along with the presence of 2D and D+G peaks confirm the formation of high-quality rGO; the absence of the D' peak indicates very few defects in the film. The 2D and D+G peaks were difficult to resolve as the use of higher acquisition time resulted in significant substrate heating and degradation. The improvement in sheet resistivity of laser annealed DLC film can be noted in Table 2. The film laser annealed at 0.3 Jcm^{-2} shows a low sheet resistivity of $0.6\text{ k}\Omega/\square$. The LIRGO patterned on flexible substrate is ideal for wearable electronics applications. The heating caused due to the laser was spatially and temporally confined; no substrate degradation was observed. The use of a shadow mask and a UV laser resulted in high resolution and a minimum flow of heat to the shadowed regions, resulting in high-quality patterned graphene in the exposed regions during masking. Researchers have previously fabricated rGO and a-C/rGO p-n junction on silicon using a similar approach¹⁴.

(b) Electrical properties of as-deposited and laser annealed Si-DLC coatings

The Tauc relation to estimate bandgap (E_g) from UV-vis measurement is given by ⁵⁸:

$$(\alpha hv)^n = A(hv - E_g) \quad (2)$$

Here, hv is the photon energy, and α is the absorption coefficient. For a direct transition, n is 0.5. The value of E_g for 21 at% Si was calculated to be 2.4 eV (Fig. 7(d)). This high-value results in very high resistivity and negligible conductivity. Studies conducted on bandgap determination of a Si-DLC thin-film report an increase of bandgap with the Si concentration. A bandgap of 2.1 eV has been reported for 15.4 at% Si-doped DLC thin films; the bandgap of non-doped DLC was reported to be close to 1 eV⁵⁹. A significant improvement in conductivity was observed after laser annealing (by six orders of magnitude) as compared to the non-annealed sample (Fig. S2 (a)); the conductivity was sustained after repeated film cycling, providing evidence of robust adhesion of the thin film to the substrate. The IV characteristics of the laser annealed Si-DLC thin film are depicted in Fig. S2 (b). Previous researchers noted a similar linear I-V curve and film graphitization on thermal annealing of 10 at% Si-DLC thin films at 500° C ⁶⁰. Figure 8 (b & d) depicts the XRD and the Raman spectrum of laser annealed Si-DLC. The peak observed at 18.7° indicates rGO formation with a higher amount of oxygen as compared to rGO obtained from laser annealing of undoped DLC. This result is also consistent with the higher I_d/I_g ratio observed after laser annealing of undoped DLC compared to laser annealing of Si-DLC, indicating a higher reduction in the case of rGO obtained from undoped DLC. Further, Table 2 demonstrates a higher value of sheet resistance obtained from rGO after laser annealing of Si-DLC at 0.3 Jcm⁻². This high value may also result from the formation of a thin SiO top layer, which acts as a dielectric layer. The formation of this layer can be advantageous for fabricating complementary metal-oxide semiconductors on flexible substrates.

Figure 9 contains the XPS spectra of the as-deposited and laser annealed Si-DLC thin films. The as-deposited and laser annealed Si-DLC thin films were shown to contain oxygen, carbon, and silicon. The carbon 1s peak can be deconvoluted into four prominent peaks that were associated with sp^2 (284.7 eV), sp^3 (285.3 eV), C=O (287 eV), and C-O (289.2 eV) ⁶¹ bonding. It is difficult to deconvolute the C-Si bond and C-C bond contributions since these binding energy values are similar. The sp^2/sp^3 ratio is two for as-deposited Si-DLC thin films, which goes up to three after laser annealing at 0.6 J/cm² (Fig. 9(b), Fig S2). Fig. 9(c) shows a low magnification optical image of a laser patterned Si-DLC film at an energy density of 0.3 J cm⁻², and Fig. 9(d) shows the sharp boundary between the laser- annealed and non-annealed regions. As

discussed previously, patterning at a high energy density leads to a film showing high wear. The laser energy of 0.3 J cm^{-2} provided optimal tribological and electrical properties.

Fig. 9 (e,f) depicts the Si 2p peak. We fitted four major peaks for SiO_x , SiC, Si-O-C, SiO_2 at binding energies of 100.2 eV, 101.2 eV, 102.2 eV, and 103.3 eV, respectively⁶²⁻⁶⁵. The as-deposited Si-DLC thin films did not show the presence of a SiO_x layer. On the other hand, thick SiO_x is present after laser annealing at energy densities greater than 0.6 J cm^{-2} (Fig. 9(f), 7(e)); this phenomenon is attributed to oxygen incorporation in the lattice. Previous studies have also hinted at the possibility of an improvement in the toughness properties due to the formation of a Si-rich transfer layer on the surface^{66,67}. However, the thick SiO_x transfer layer obtained at high laser annealing energy densities leads to a film showing high wear. This result indicates that Si-DLC thin films are unsuitable for applications involving high-energy UV irradiation. However, recent studies have indicated that a SiO_x top layer results in corrosion property enhancement on metallic substrates⁴⁵.

3. Significance of obtained results

The performance of DLC coated PE used in hip and knee implants has not been satisfactory. Diamond Rota Gliding (Implant Design, Switzerland) named DLC-PE based knee implant was markedly commercialized in 2001, which eventually suffered wear, partial delamination, and inadequate bone ingrowth. Later, the Adamante (Biomécanique, France) femoral head implant based on DLC-linked PE was clinically studied over a decade. Initially, they underwent osteolysis (bone resorption) and cellular inflammation, while an obligatory replacement was required in later years⁶⁸. However, few studies systematically have characterized DLC film growth on PE substrates. In this study, both the DLC coated and Si-DLC coated HDPE substrates showed no signs of visible damage until $\sim 32 \text{ MPa}$ of contact stress with the diamond indenter, well above the average theoretical contact stress that knee and hip joints undergo ($\sim 10 \text{ MPa}$)⁶⁹. The authors expect that similar mechanical and adhesion properties as well as the tribological behavior of the a-C coatings as obtained on HDPE would also be achievable on HXLPE substrates which are currently preferred implant materials due to their improved wear resistance as compared to conventional UHMWPE substrates. Similar results have been reported by Rothhammer et al. for a-C films on UHMWPE substrates⁷⁰.

Few studies have demonstrated the capability of scaling up rGO on flexible polymeric substrates with a high degree of control. Recently, rGO flakes fabricated by reduction of GO using a hydrogen iodide vapor on PET showed superior

electrical properties with a sheet resistivity of $120 \Omega/\square$ ⁷¹. However, residual functional groups after reduction, as demonstrated by Raman and FTIR spectroscopy, altered the electrical and optical properties of the PET/rGO films. Another popular approach has been a roll-to-roll technique adaptable for mass production using Sn²⁺/ethanol for reduction at 50° C¹⁸. The rGO films synthesized by laser irradiation on HDPE substrates exhibited properties close to those reported in these studies. The novel laser-based rGO fabrication discussed in this manuscript will contribute towards improved performance, thermal stability, and durability of PE for flexible electronic and biomedical sensing applications.

Conclusions

In conclusion, 21 at% Si-DLC thin films (250 nm thick) deposited by PECVD showed better adhesion properties compared to pristine DLC thin films deposited by PLD on HDPE substrates that were modified with F-RIE. The Si-DLC thin films had a grain size of ~100 nm as calculated from SEM and AFM data. The sp³ content and stress reduction achieved as a result of Si incorporation were not able to prevent thin film cracking above a load of ~11 mN. This cracking was avoided by increasing the sp² content of the thermally stable Si-DLC thin film by the PLA technique. Appropriate levels of adhesion, hardness, lubricity, electrical conductivity, and hydrophobicity can be tailored by doping DLC with Si and performing UV laser annealing to modify the sp²/sp³ content of the thin film below an energy density of 0.3 J cm⁻². A laser annealing density greater than 0.6 J cm⁻² resulted in the formation of a thick SiO_x transfer layer, which showed improved toughness and increased wear rate. This study successfully demonstrated the utility of plasma- and laser-based processing techniques for deposition and structural modification of carbon thin films on thermally sensitive HDPE substrates. Further, these Si-DLC coated HDPE substrates can also be implemented for gas barrier⁴ and packaging applications.

Author contributions

Pratik Joshi: Formal analysis, Writing - original draft, conducted the materials synthesis, Raman spectroscopy, HRSEM imaging, X-ray diffraction. **Parand Riley:** UV-vis, FTIR. **Shubhangi Shukla:** Writing - original draft, **Nayna Khosla:** IV measurements **Roger J. Narayan:** Supervision, conceived the project, and funding. **Jagdish Narayan:** Supervision, conceived the project, and funding.

Conflict of interest

The authors declare that they have no known competing financial interests or personal relationships that could have appeared to influence the work reported in this paper.

Acknowledgments

The authors would like to thank William Kiether for his assistance with the deposition of the Si-DLC thin films and Warren Denning at Anton Paar for his assistance with micro-scratch adhesion testing. The authors would also like to acknowledge the support of National Science Foundation Award #1836767. This work was performed in part at the NCSU Nanofabrication Facility (NNF), a member of the North Carolina Research Triangle Nanotechnology Network (RTNN), which is supported by the National Science Foundation (Grant ECCS-1542015) as part of the National Nanotechnology Coordinated Infrastructure (NNCI). This work was performed in part at the Analytical Instrumentation Facility (AIF) at North Carolina State University, which is supported by the State of North Carolina and the National Science Foundation (award number ECCS-2025064). The AIF is a member of the North Carolina Research Triangle Nanotechnology Network (RTNN), a site in the National Nanotechnology Coordinated Infrastructure (NNCI).

Table 1: Summary of data obtained from scratch testing.

Material	L_{c1} (mN)	Avg	L_{c2} (mN)	Avg
DLC on HDPE (No RIE)	0		0	
DLC on HDPE (RIE)	8.19,8.45	8.32	9.85,10.43	10.14
Si-DLC on HDPE (PECVD)	10.57,12.93	11.75	40.43,44.99	42.71
Laser annealed Si-DLC on HDPE (PECVD)	NA	NA	>100	>100

Table 2: Sheet resistivity of carbon thin films on HDPE substrate

Material	Treatment	Sheet resistivity ($k\Omega/\square$)
DLC (F-RIE HDPE)	As-deposited	648
	LA at 0.1 Jcm^{-2}	326
	LA at 0.3 Jcm^{-2}	0.6
Si DLC	As-deposited	>700
	LA at 0.3 Jcm^{-2}	37
	LA at 0.6 Jcm^{-2}	26

Figures:

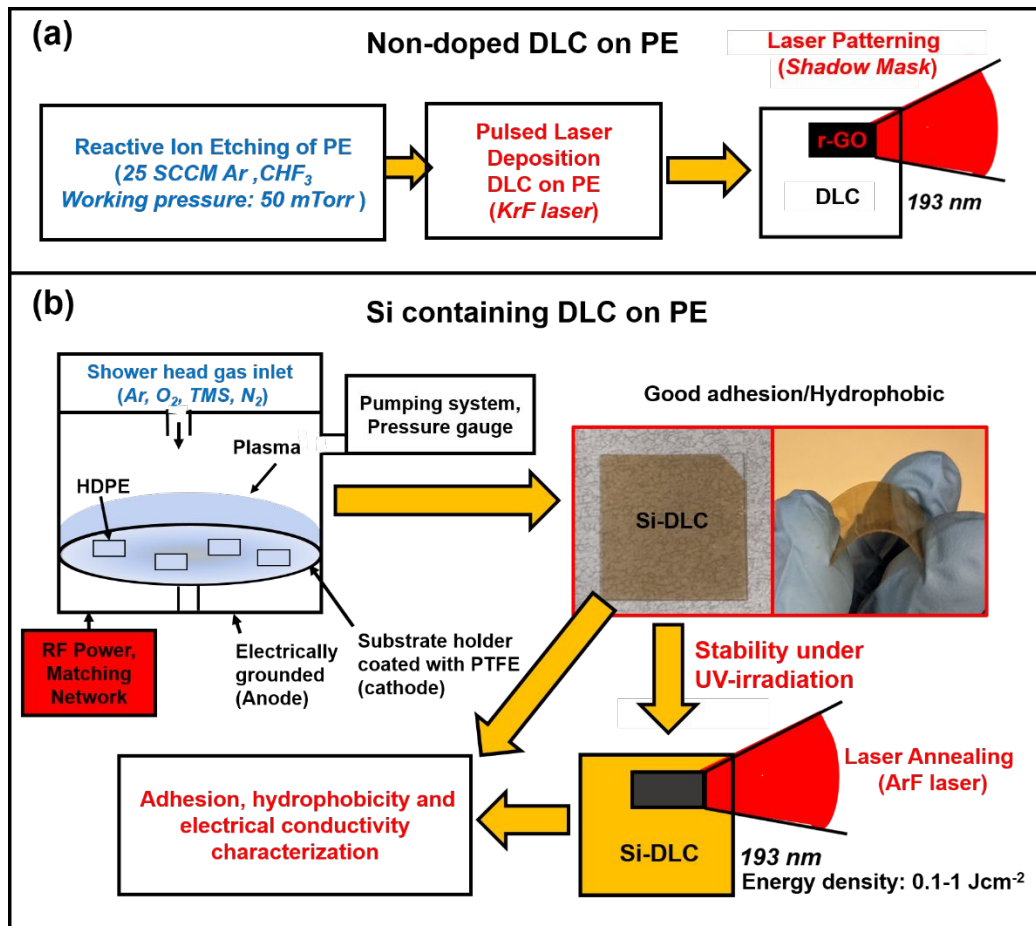


Fig. 1. Schematic depicting: (a) DLC deposition on fluorine-modified polyethylene substrate using the PLD system followed by UV laser writing of reduced graphene oxide for wearable electronics applications, and (b) Si-containing DLC deposition on HDPE using the PECVD system for biomedical implant applications; laser annealing of the Si-containing DLC using an ArF laser is also shown.

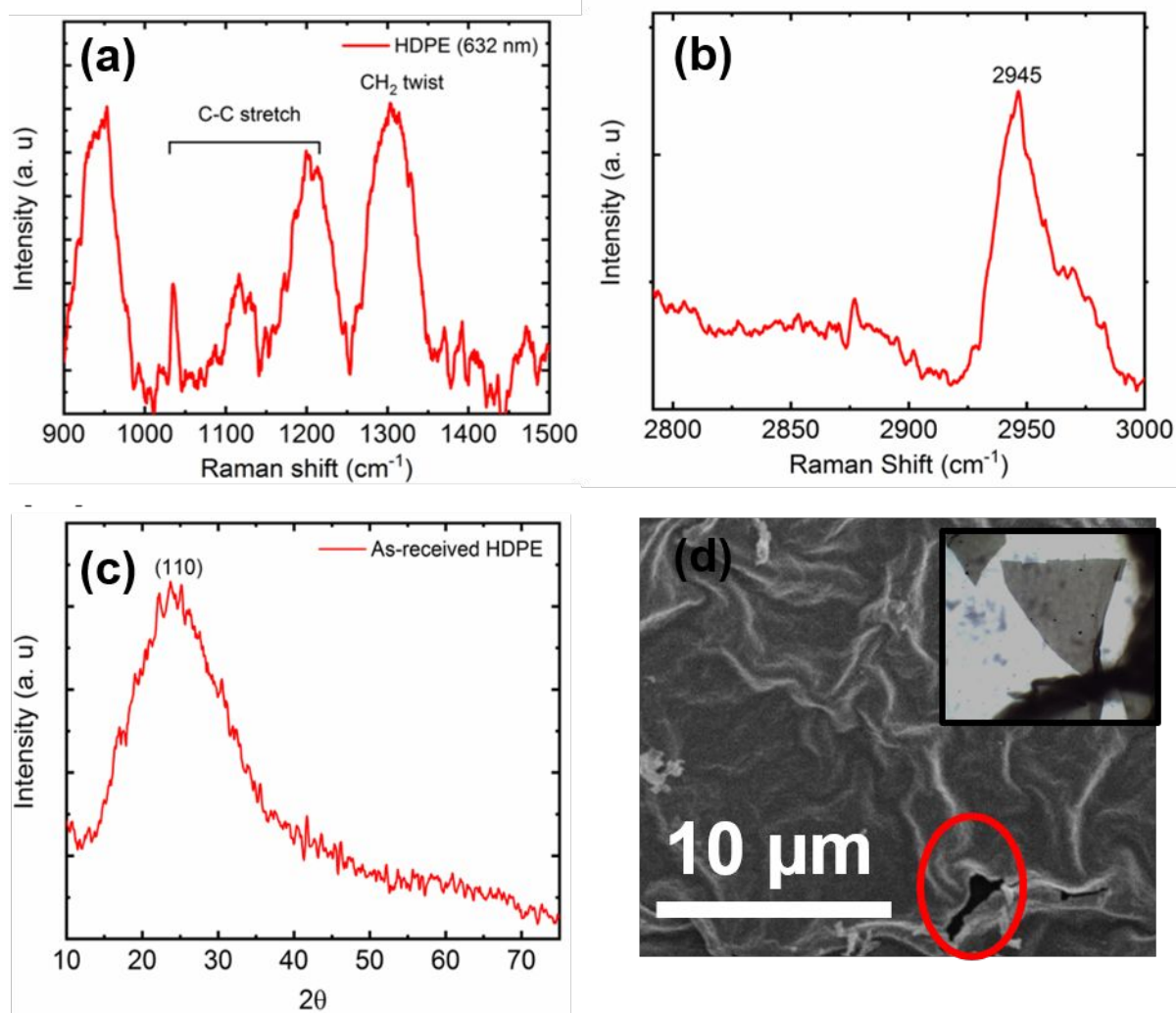


Fig. 2. (a, b) Raman spectra of HDPE acquired using the 632 nm laser, (c) XRD spectrum of as-received HDPE, and (d) SEM micrograph of laser annealed DLC film tear on HDPE deposited by PLD without F-RIE treatment; the inset shows an optical micrograph of the delaminated coating.

As-received HDPE After reactive ion etching

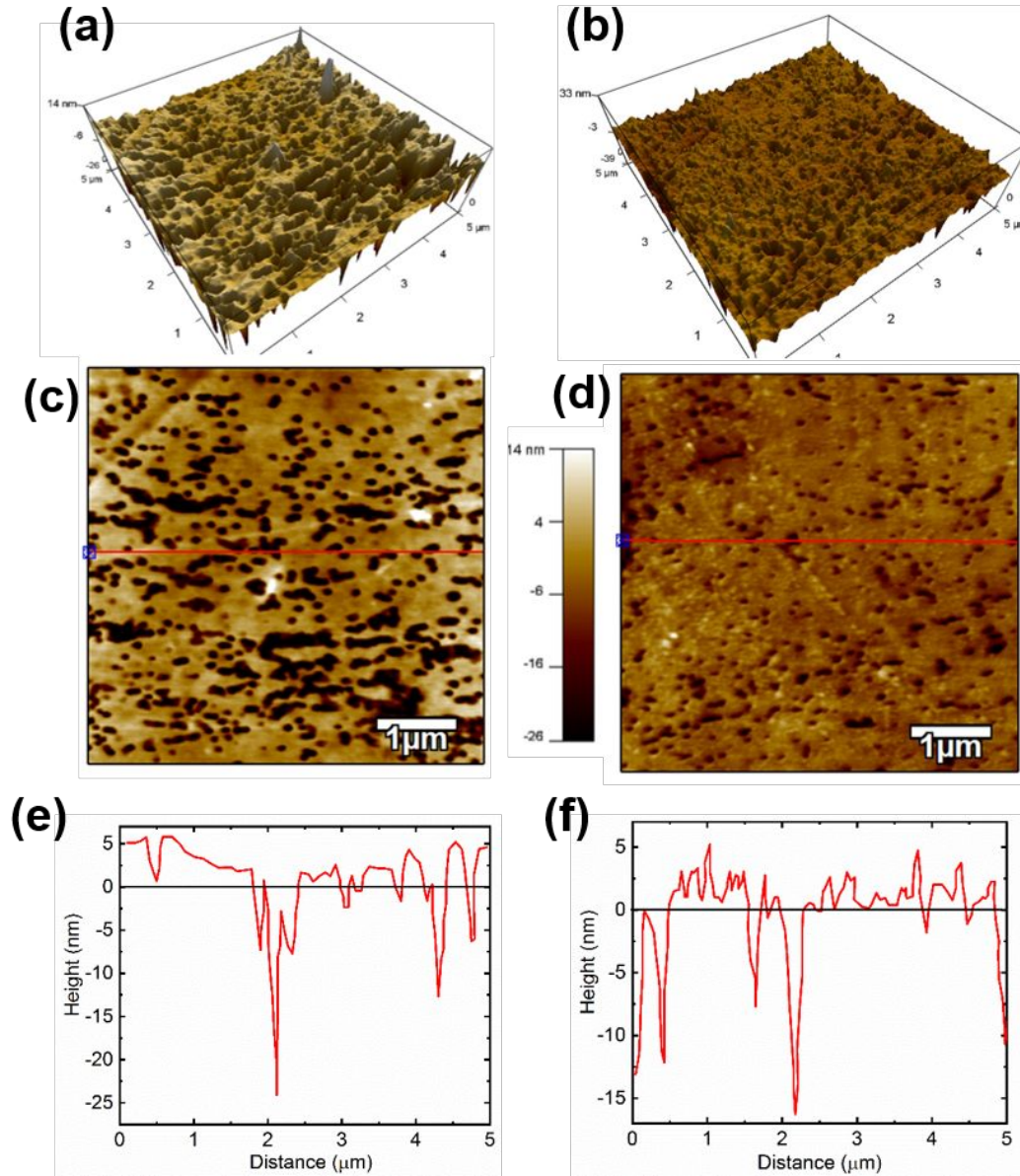


Fig. 3. 3D Surface roughness scan of (a) as-received HDPE and (b) after F-RIE of HDPE; 2D surface roughness scan of (c) as-received HDPE and (d) after F-RIE of HDPE. (e) Depth vs. distance profile of (c) and (f) depth vs. distance profile of (d).

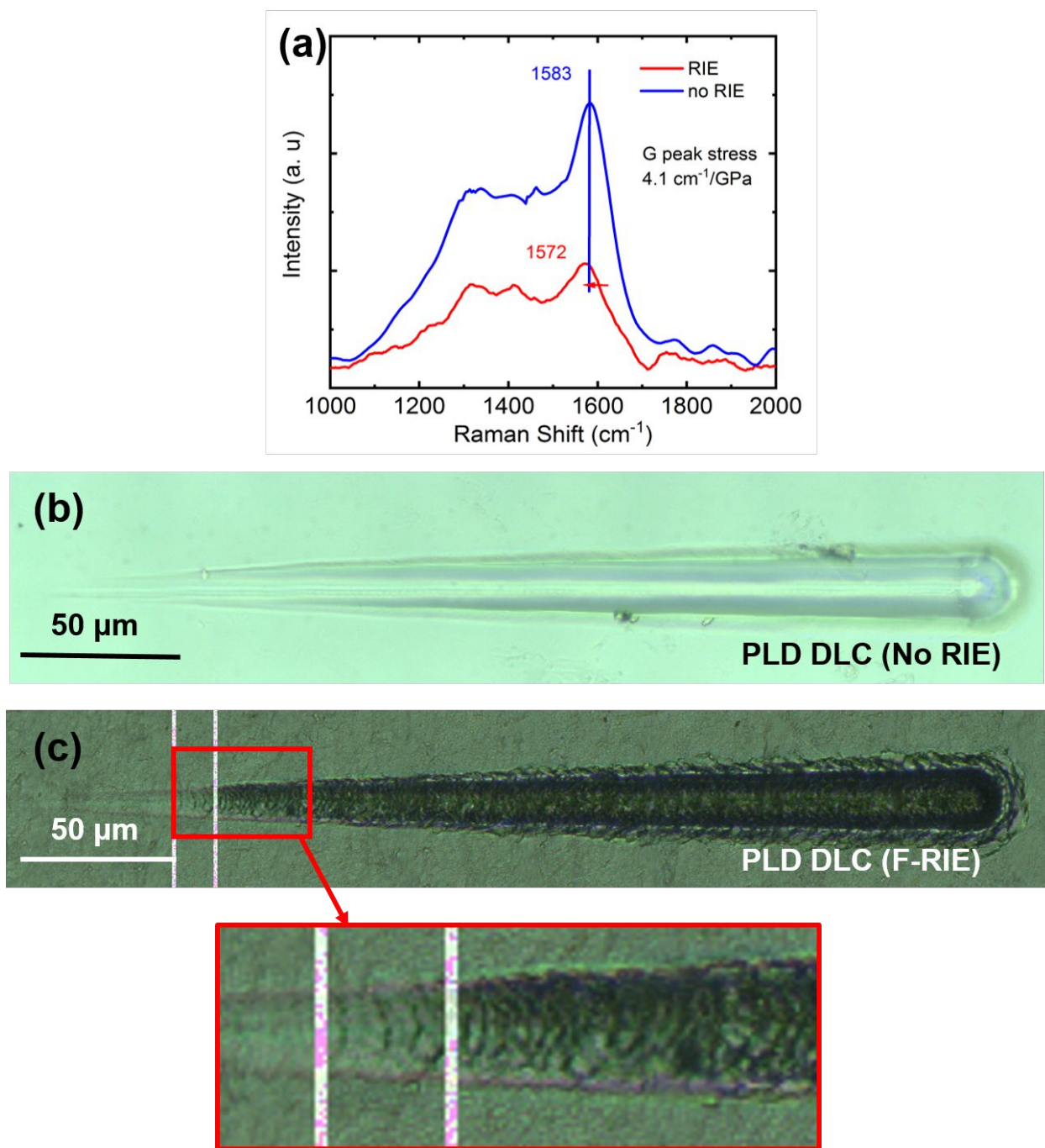


Fig. 4. (a) Raman spectra of DLC deposited on HDPE with and without F-RIE modification (red arrow depicting the G peak shift). Optical micrograph after scratch test on (b) HDPE coated with DLC, and (c) F-RIE treated HDPE coated with DLC; the magnified image of the visible cracks is shown in the red box.

Si-DLC on HDPE by PECVD

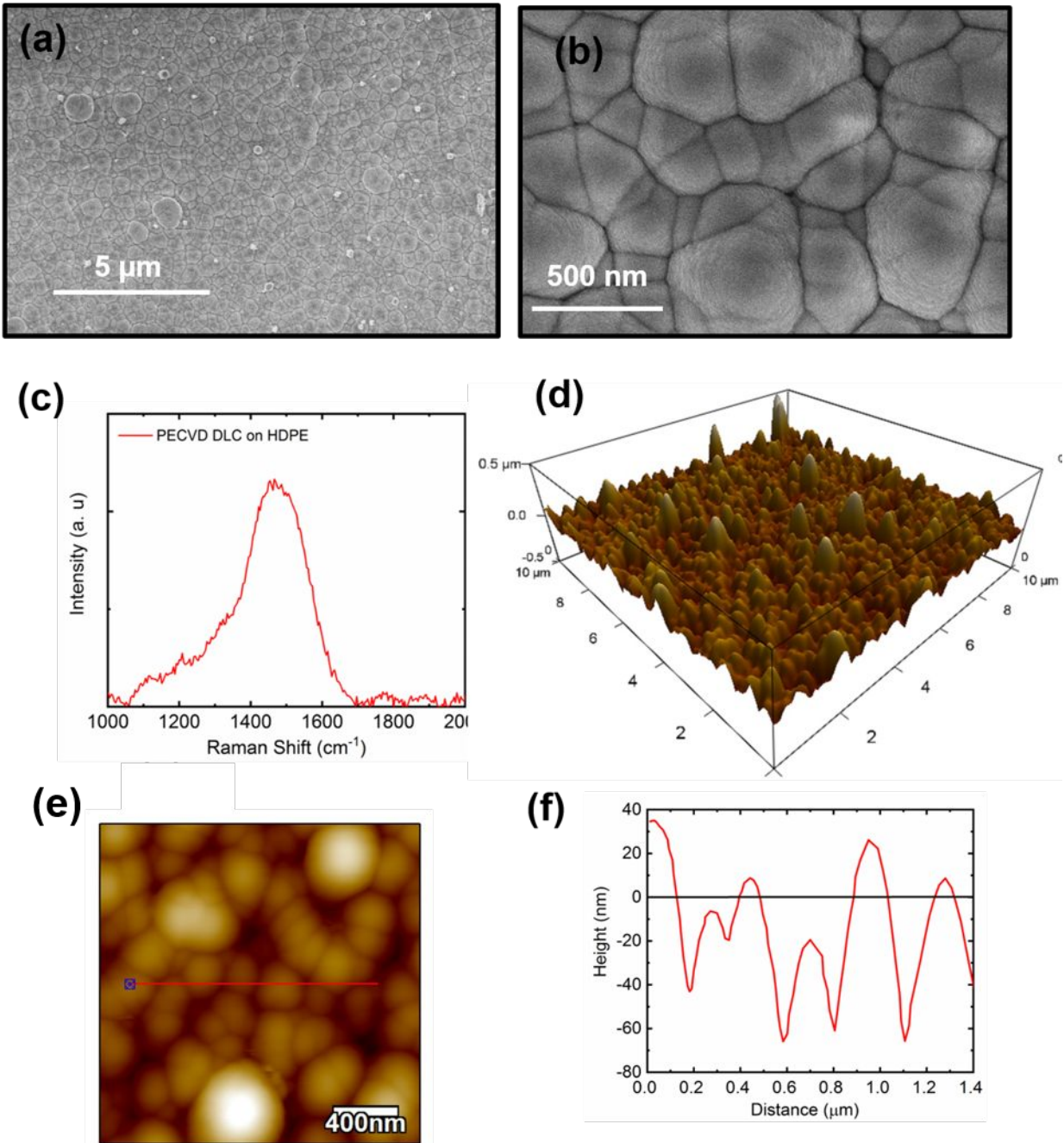


Fig. 5. SEM image of an as-deposited 500 nm Si-DLC thin film at (a) low magnification and (b) high magnification; (c) Raman spectrum of Si-DLC on HDPE, (d) 3D AFM surface roughness plot of a 200 nm Si-DLC thin film; (e) 2D roughness plot and (f) height vs. distance along the red line shown in (d).

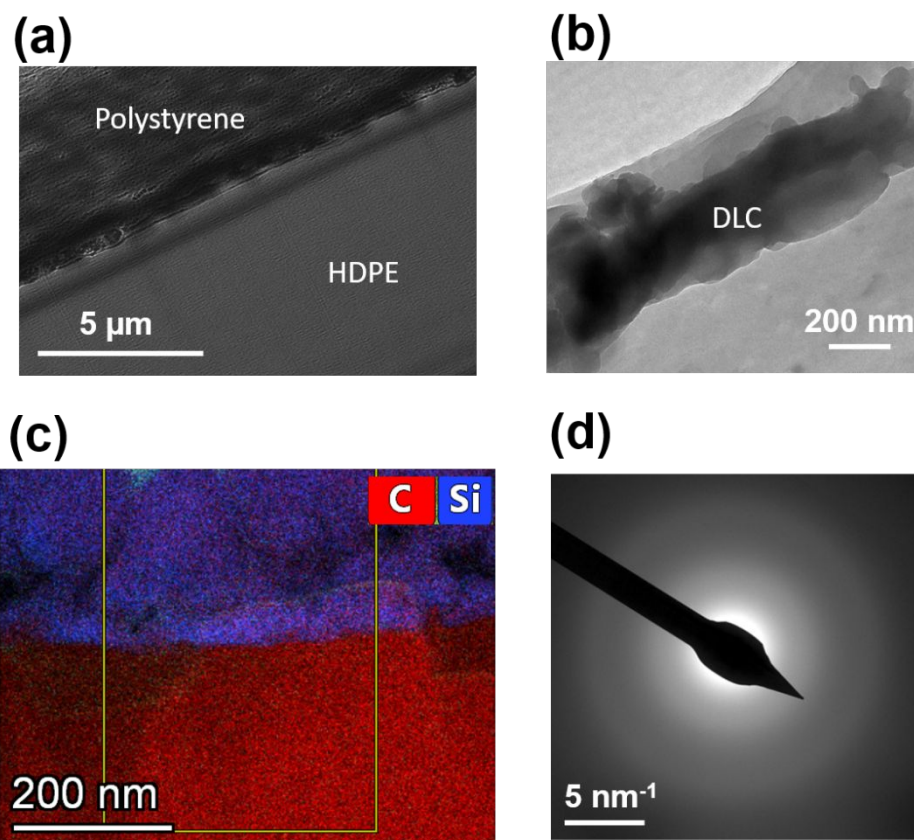


Fig. 6. (a) TEM micrograph of low magnification image of the sample configuration, (b) TEM micrograph of Si-DLC thin film (dark contrast), (c) EDS at Si-DLC and HDPE interface, and (d) SAED pattern from the Si-DLC thin film.

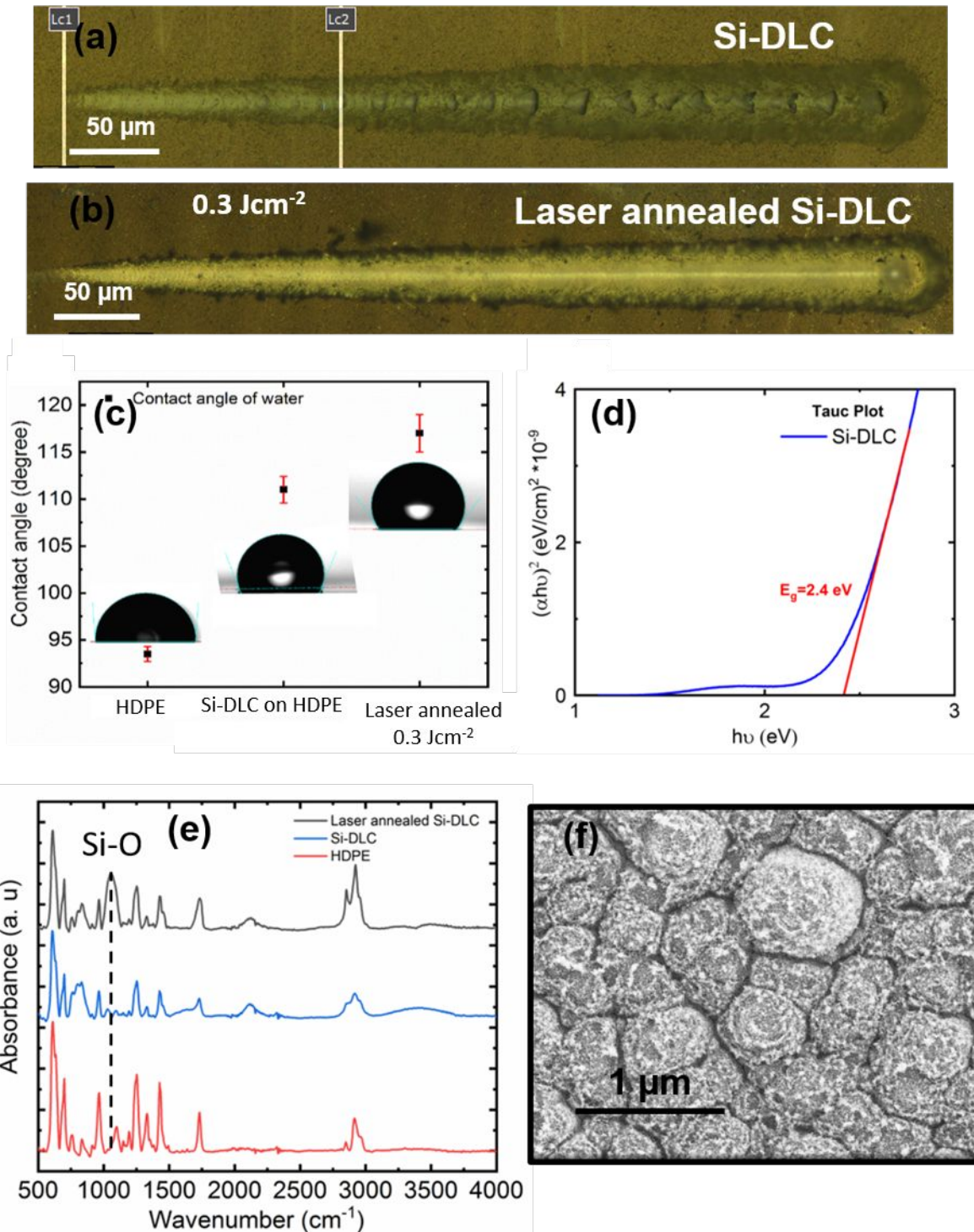


Fig. 7. Optical micrograph after scratch test on HDPE (a) coated with Si-DLC and (b) laser annealed Si-DLC, (c) contact angle of water on as-deposited and laser annealed DLC, (d) Tauc plot of Si-DLC thin film, (e) FTIR showing the presence of Si-O bonds after laser annealing at 0.6 J cm⁻², and (f) HRSEM of graphitic/SiO_x layer formed on the surface after laser annealing Si-DLC at 0.6 J cm⁻².

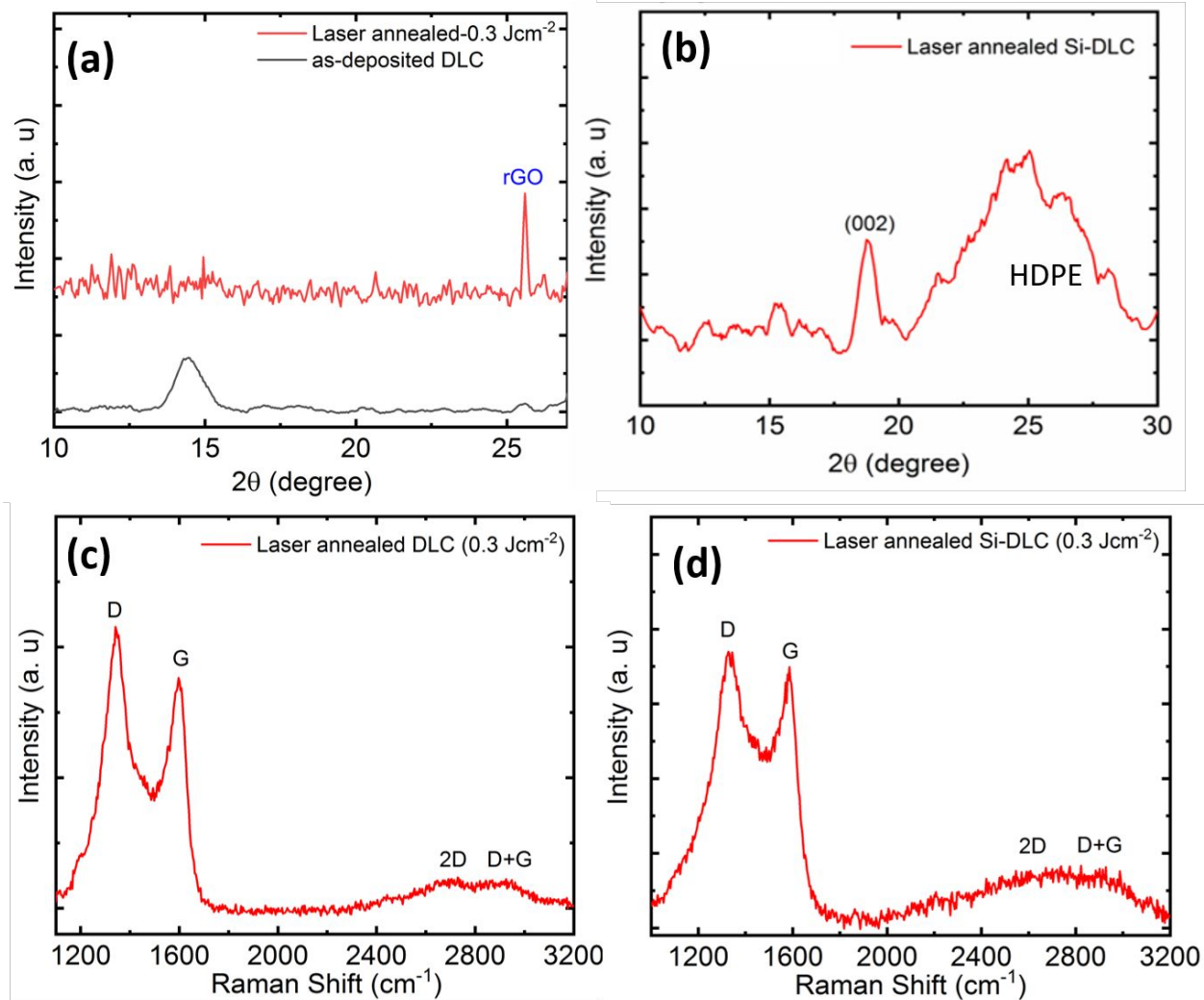


Fig. 8. Raman and XRD spectra of rGO film obtained after laser irradiation at 0.3 Jcm^{-2} on (a, c) DLC and (b, d) Si-DLC.

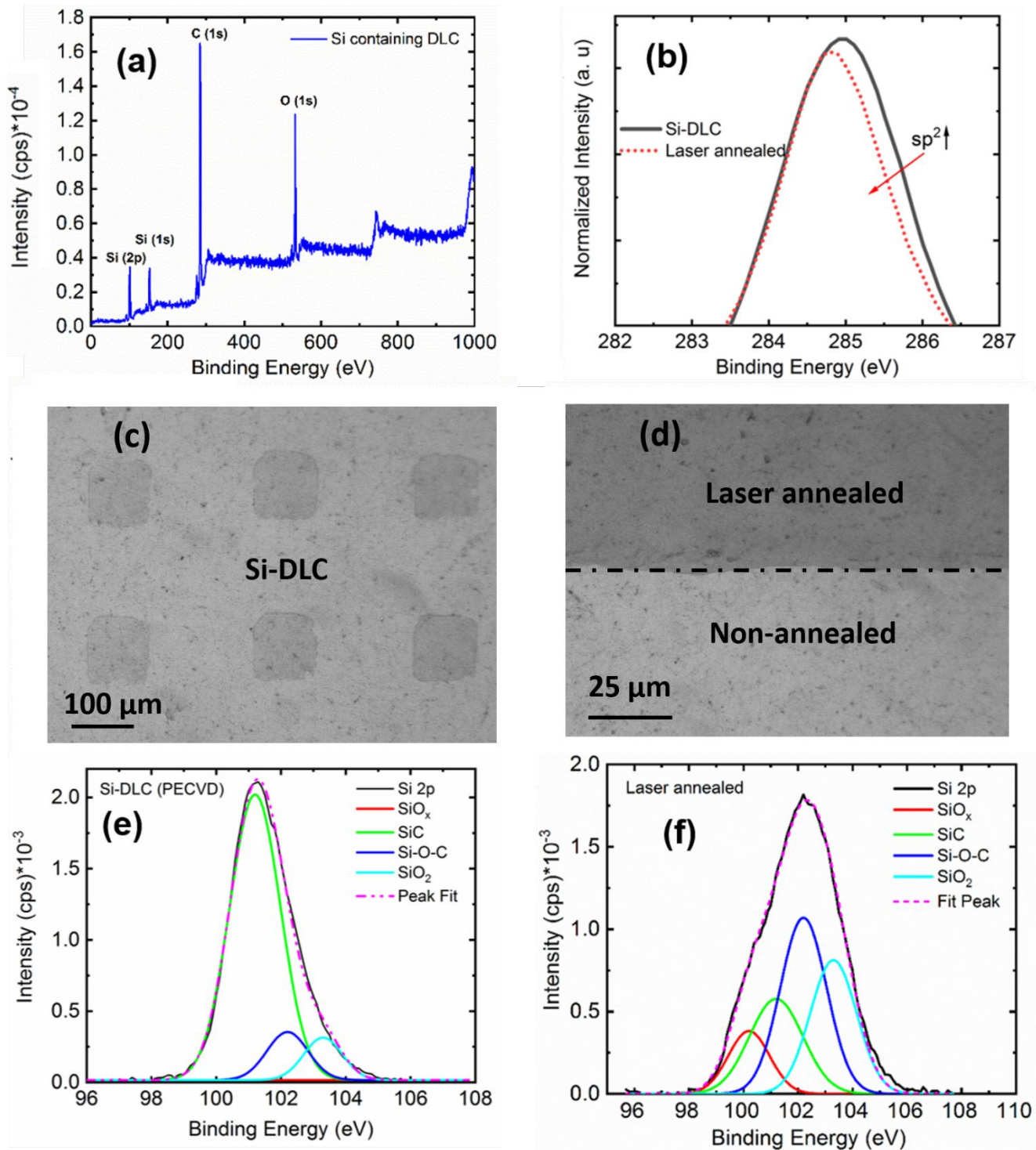


Fig. 9. (a) The XPS spectrum of Si-DLC and (b) comparison of C1s spectra of laser annealed (0.6 J cm^{-2}) and non-laser annealed Si-DLC. (c,d) Low and high magnification optical micrograph of laser patterned Si-DLC films; Si 2p fitting for (e) Si-DLC and (f) laser-annealed (0.6 J cm^{-2}) Si-DLC films.

References

- 1 Y.-N. Song, R.-J. Ma, L. Xu, H.-D. Huang, D.-X. Yan, J.-Z. Xu, G.-J. Zhong, J. Lei and Z.-M. Li, *ACS Appl. Mater. Interfaces*, 2018, **10**, 41637–41644.
- 2 N. C. Paxton, M. C. Allenby, P. M. Lewis and M. A. Woodruff, *Eur. Polym. J.*, 2019, **118**, 412–428.
- 3 S. Affatato, G. Bersaglia, M. Rocchi, P. Taddei, C. Fagnano and A. Toni, *Biomaterials*, 2005, **26**, 3259–3267.
- 4 P. R. Riley, P. Joshi, S. A. Machekposhti, R. Sachan, J. Narayan and R. J. Narayan, *Polym. 2021, Vol. 13, Page 3543*, 2021, **13**, 3543.
- 5 T. Sato, Y. Nakashima, K. Komiyama, T. Yamamoto, G. Motomura and Y. Iwamoto, *J. Arthroplasty*, 2016, **31**, 1228–1232.
- 6 J. I. Oate, M. Comin, I. Braceras, A. Garcia, J. L. Viviente, M. Brizuela, N. Garagorri, J. L. Peris and J. I. Alava, *Surf. Coatings Technol.*, 2001, **142–144**, 1056–1062.
- 7 R. K. Roy and K.-R. Lee, The Japanese Society for Biomaterials, and The Australian Society for Biomaterials and the Korean Society for Biomaterials 83.1 (2007): 72-84.
- 8 T. J. Smith, A. Galm, R. Wells, S. Pedersen, A. E. Goodship and G. W. Blunn, In *Transactions-7th World Biomaterials Congress*. 2004.
- 9 E. Alakoski, V.-M. Tiainen, A. Soininen and Y. T. Konttinen, *Open Orthop. J.*, 2008, **2**, 43.
- 10 P. C. Piconi, V. De Santis and G. Maccauro, *Joints* 5(04) (2017): 224-228.
- 11 S. Jasmee, G. Omar, N. A. B. Masripan, A. A. Kamarolzaman, A. S. Ashikin and F. Che Ani, *Mater. Res. Express*, 2018, **5**, 096304.
- 12 Y. Fu, J. Hansson, Y. Liu, S. Chen, A. Zehri, M. K. Samani, N. Wang, Y. Ni, Y. Zhang, Z. Bin Zhang, Q. Wang, M. Li, H. Lu, M. Sledzinska, C. M. S. Torres, S. Volz, A. A. Balandin, X. Xu and J. Liu, *2D Mater.*, 2019, **7**, 012001.
- 13 D. Ma, Y. Su, T. Tian, H. Yin, C. Zou, T. Huo, N. Hu, Z. Yang and Y. Zhang, *ACS Appl. Mater. Interfaces*, 2020, **12**, 37418–37426.
- 14 Z. Xing, Y. Zheng, Z. Yan, Y. Feng, Y. Xiao, J. Yu, H. Guan, Y. Luo, Z. Wang, Y. Zhong and Z. Chen, *Sensors Actuators B Chem.*, 2019, **281**, 953–959.
- 15 M. Xu, Y. Zhu, S. Gao, Z. Zhang, Y. Gu and X. Liu, *ACS Appl. Nano Mater.*, 2021, **4**, 12442–12452.
- 16 S. Kasturi, Y. Eom, S. R. Torati and C. G. Kim, *J. Ind. Eng. Chem.*, 2021, **93**, 186–195.

- 17 A. Habermehl, C. R. Nieto, C. Müller, G. H. Sosa, H. A. R. Tito, M. E. Q. Caceda and S. Beck, *Appl. Opt. Vol. 56, Issue 28, pp. 7774-7780*, 2017, **56**, 7774–7780.
- 18 J. Ning, L. Hao, M. Jin, X. Qiu, Y. Shen, J. Liang, X. Zhang, B. Wang, X. Li, L. Zhi, J. Ning, L. Hao, M. Jin, X. Qiu, Y. Shen, J. Liang, X. Zhang, B. Wang, X. Li and L. Zhi, *Adv. Mater.*, 2017, **29**, 1605028.
- 19 S. Gupta, P. Joshi and J. Narayan, *Carbon N. Y.*, 2020, **170**, 327–337.
- 20 P. Joshi, A. Haque, S. Gupta, R. J. Narayan and J. Narayan, *Carbon N. Y.*, 2021, **171**, 739–749.
- 21 J. Narayan, A. Bhaumik, S. Gupta, P. Joshi, P. Riley and R. J. Narayan, *Carbon N. Y.*, 2021, **176**, 558–568.
- 22 R. Sachan, S. Gupta and J. Narayan, *ACS Appl. Mater. Interfaces*, 2020, **12**, 1330–1338.
- 23 P. R. Riley, P. Joshi, H. Penchev, J. Narayan and R. J. Narayan, *Cryst. 2021, Vol. 11, Page 1308*, 2021, **11**, 1308.
- 24 N. Dwivedi, S. Kumar, H. K. Malik, Govind, C. M. S. Rauthan and O. S. Panwar, *Appl. Surf. Sci.*, 2011, **257**, 6804–6810.
- 25 P. Joshi, P. Riley, S. Gupta, R. Narayan and J. Narayan, *Nanotechnology*, , DOI:10.1088/1361-6528/AC1097.
- 26 J. Narayan, P. Joshi, J. Smith, W. Gao, W. J. Weber and R. J. Narayan, *Carbon N. Y.*, 2022, **186**, 253–261.
- 27 A. Bendavid, P. J. Martin, C. Comte, E. W. Preston, A. J. Haq, F. S. Magdon Ismail and R. K. Singh, *Diam. Relat. Mater.*, 2007, **16**, 1616–1622.
- 28 R. Hauert, *Diam. Relat. Mater.*, 2003, **12**, 583–589.
- 29 D. Bociaga, A. Sobczyk-Guzenda, P. Komorowski, J. Balcerzak, K. Jastrzebski, K. Przybyszewska and A. Kaczmarek, *Nanomaterials*, , DOI:10.3390/NANO9060812.
- 30 N. V. G. Sakhrani and C. S. University, North Carolina State University, 1997.
- 31 S. Movahed, A. K. Nguyen, P. L. Goering, S. A. Skoog and R. J. Narayan, *Biointerphases*, 2020, **15**, 041007.
- 32 C. B. Fischer, M. Rohrbeck, S. Wehner, M. Richter and D. Schmeißer, *Appl. Surf. Sci.*, 2013, **271**, 381–389.
- 33 H. Sato, M. Shimoyama, T. Kamiya, T. Amari, S. Aic, T. Ninomiya, H. W. Siesler and Y. Ozaki, *J. Appl. Polym. Sci.*, 2002, **86**, 443–448.
- 34 Y. Hiejima, T. Kida, K. Takeda, T. Igarashi and K. hei Nitta, *Polym. Degrad. Stab.*, 2018, **150**, 67–72.
- 35 Q. Wei and J. Narayan, *Int. Mater. Rev.*, 2000, **45**, 133–164.
- 36 K. Kyzioł, P. Jabłoński, W. Niemiec, J. Prazuch, D. Kottfer, A. Łętocha and Ł. Kaczmarek, *Appl. Phys. A 2020 1269*, 2020, **126**, 1–13.
- 37 S. M. Carley, Doctoral dissertation, University of Leeds, 2017.

- 38 I. S. Trakhtenberg, O. M. Bakunin, I. N. Korneyev, S. A. Plotnikov, A. P. Rubshtein and K. Uemura, *Diam. Relat. Mater.*, 2000, **9**, 711–714.
- 39 A. Voss, S. R. Stateva, J. P. Reithmaier, M. D. Apostolova and C. Popov, *Surf. Coatings Technol.*, 2017, **321**, 229–235.
- 40 K. H. Yang, P. Joshi, K. B. Rodenhausen, A. V. Sumant, S. A. Skoog and R. J. Narayan, *Mater. Lett.*, 2021, **295**, 129823.
- 41 H. Puliyalil and U. Cvelbar, *Nanomater. 2016, Vol. 6, Page 108*, 2016, **6**, 108.
- 42 G. Q. Yu, B. K. Tay, Z. Sun and L. K. Pan, *Appl. Surf. Sci.*, 2003, **219**, 228–237.
- 43 J. K. Shin, C. S. Lee, K. R. Lee and K. Y. Eun, *Appl. Phys. Lett.*, 2001, **78**, 631.
- 44 A. Moreno-Barcenas, J. M. Alvarado-Orozco, J. M. G. Carmona, G. C. Mondragon-Rodriguez, J. Gonzalez-Hernandez and A. Garcia-Garcia, *Surf. Coatings Technol.*, 2018, **374**, 327–337.
- 45 B. Ollivier and A. Matthews, *J. Adhes. Sci. Technol.*, 1994, **8**, 651–662.
- 46 R. Matsumoto, K. Sato, K. Ozeki, K. Hirakuri and Y. Fukui, *Diam. Relat. Mater.*, 2008, **17**, 1680–1684.
- 47 A. Catena, S. Agnello, L. M. Rösken, H. Bergen, E. Recktenwald, F. Bernsmann, H. Busch, M. Cannas, F. M. Gelardi, B. Hahn, S. Wehner and C. B. Fischer, *Carbon N. Y.*, 2016, **96**, 661–671.
- 48 Y. Namba, T. Mōri and T. Mori, *Diamondlike Carbon J. Appl. Phys.*, 1985, **3**, 2953.
- 49 M. S. de Luna, M. Galizia, J. Wojnarowicz, R. Rosa, W. Lojkowski, C. Leonelli, D. Acierno and G. Filippone, *Express Polym. Lett.*, 2016, **8**, 362–372.
- 50 M. H. Ahmed, J. A. Byrne and W. Ahmed, *Diam. Relat. Mater.*, 2015, **55**, 108–116.
- 51 K. Kyzioł, P. Jabłoński, W. Niemiec, J. Prazuch, D. Kottfer, Aneta Łętocha and Ł. Kaczmarek, *Appl. Phys. A*, 2020, **126**, 751.
- 52 P. R. Riley and R. J. Narayan, *Curr. Opin. Biomed. Eng.*, 2021, **17**, 100262.
- 53 P. T. Phuong, S. Oliver, J. He, E. H. H. Wong, R. T. Mathers and C. Boyer, *Biomacromolecules*, 2020, **21**, 5241–5255.
- 54 M. Castellino, V. Stolojan, A. Virga, M. Rovere, K. Cabiale, M. R. Galloni and A. Tagliaferro, *Anal. Bioanal. Chem.*, 2013, **405**, 321–329.
- 55 A. Grill and V. Patel, *Appl. Phys. Lett.*, 1998, **60**, 2089.
- 56 S. C. Ray, B. Bose, J. W. Chiou, H. M. Tsai, J. C. Jan, K. Kumar, W. F. Pong, D. DasGupta, G. Fanchini and A. Tagliaferro, *J. Mater. Res.*, 2004, **19**, 1126–1132.

- 57 J. Y. Lin and B. X. Wang, *Adv. Mater. Sci. Eng.* 2014
- 58 S. Majeed, K. Siraj, S. Naseem, M. F. Khan, M. Irshad, H. Faiz and A. Mahmood, *Mater. Res. Express*, 2017, **4**, 076403.
- 59 M. S. Alam, N. Mukherjee and S. F. Ahmed, *AIP Conf. Proc.*, 2018.
- 60 T. I. T. Okpalugo, P. D. Maguire, A. A. Ogwu and J. A. D. McLaughlin, *Diam. Relat. Mater.*, 2004, **13**, 1549–1552.
- 61 D. J. E. Costa, J. C. S. Santos, F. A. C. Sanches-Brandão, W. F. Ribeiro, G. R. Salazar-Banda and M. C. U. Araujo, *J. Electroanal. Chem.*, 2017, **789**, 100–107.
- 62 Š. Meškiniš, S. Tamulevičius, V. Kopustinskas, M. Andrulėvičius, A. Guobiene, R. Gudaitis and I. Liutviniene, *Thin Solid Films*, 2007, **515**, 7615–7618.
- 63 Š. Meškiniš, A. Vasiliauskas, M. Andrulėvičius, D. Peckus, S. Tamulevičius and K. Viskontas, *Mater. 2020, Vol. 13, Page 1003*, 2020, **13**, 1003.
- 64 M. Veres, M. Koós, S. Tóth, M. Füle, I. Pócsik, A. Tóth, M. Mohai and I. Bertóti, *Diam. Relat. Mater.*, 2005, **14**, 1051–1056.
- 65 S.-Y. Jing, H.-J. Lee and C. K. Choi, *J. Korean Phys. Soc.*, 2002, **41**, 769–773.
- 66 C. Jongwannasiri, S. Yoshida, S. Watanabe, C. Jongwannasiri, S. Yoshida and S. Watanabe, *Mater. Sci. Appl.*, 2019, **10**, 170–185.
- 67 M. G. Kim, K. R. Lee and K. Y. Eun, *Surf. Coatings Technol.*, 1999, **112**, 204–209.
- 68 A. M. Pinto, A. T. Pereira and I. C. Gonçalves, *Carbon Biomaterials*, Elsevier, Fourth Edi., 2020.
- 69 R. A. Brand, *Iowa Orthop. J.*, 2005, **25**, 82.
- 70 B. Rothhammer, K. Neusser, M. Marian, M. Bartz, S. Krauß, T. Böhm, S. Thiele, B. Merle, R. Detsch and S. Wartzack, *Polym. 2021, Vol. 13, Page 1952*, 2021, **13**, 1952.
- 71 A. Habermehl, C. R. Nieto, C. Müller, G. H. Sosa, H. A. R. Tito, M. E. Q. Caceda and S. Beck, *Appl. Opt. Vol. 56, Issue 28, pp. 7774-7780*, 2017, **56**, 7774–7780.